Final Draft

of the original manuscript

Gruber, D.; Kiefer, D.; Rössler, R.; Beckmann, F.; Tkadletz, M.;
Klünsner, T.; Czettl, C.; Keckes, J.; Gibmeier, J.:

20 Hz synchrotron X-ray diffraction analysis in laser-pulsed WC-Co hard metal reveals oscillatory stresses and reversible composite plastification.

In: International Journal of Refractory Metals and Hard Materials.
Vol. 82 (2019) 121 - 128.
First published online by Elsevier: 10.04.2019

https://dx.doi.org/10.1016/j.ijrmhm.2019.04.004

20 Hz Synchrotron X-ray Diffraction Analysis in Laser-Pulsed WC-Co Hard Metal Reveals Oscillatory Stresses and Reversible Composite Plastification

David P. Gruber[1,2,a], Dominik Kiefer[3,a], Ralf Rössler[3], Felix Beckmann[4], Michael Tkadletz[1], Thomas Klünsner[5], Christoph Czettl[6], Jozef Keckes[1,2,*], Jens Gibmeier[3]

[1] *Department of Materials Science, Montanuniversität Leoben, 8700 Leoben, Austria*
[2] *Erich Schmid Institute of Materials Science, Austrian Academy of Sciences, 8700 Leoben, Austria*
[3] *Institute of Applied Materials, Karlsruhe Institute of Technology, 76131 Karlsruhe, Germany*
[4] *Institute of Materials Research, Helmholtz-Zentrum Geesthacht (HZG), 21502 Geesthacht, Germany*
[5] *Materials Center Leoben Forschung GmbH, 8700 Leoben, Austria*
[6] *Ceratizit Austria GmbH, 6600 Breitenwang*

Abstract

The lifetime of WC-Co inserts used in cutting processes, such as milling, is limited by millisecond temperature and mechanical pulses, which occur as a result of interrupted tool-workpiece contact, thermal fatigue and wear. In the current work, synchrotron X-ray diffraction (XRD) was used in conjunction with a pulsed laser heating set-up to characterise the time-dependent development of stresses and microstructure in locally irradiated WC-Co inserts coated by chemical vapour deposition with 6.5 and 3.5 µm thick TiCN and α-Al_2O_3 films, respectively. Diffraction data from the WC-Co phase were used to evaluate the time and temperature-dependent evolution of in-plane stresses, thermal strains and integral breadths of WC diffraction peaks in experiments with a single and five successive laser shocks applied within 2.2 and 20 seconds, respectively, using a laser spot diameter of ~5.8 mm and an X-ray beam size of 1 × 1 mm^2. The laser heating induces the formation of compressive stresses in the inserts' substrates. Above a temperature of ~750°C, at the onset of WC-Co composite plastification, compressive stresses relax and then vanish in WC at the maximal applied temperature of ~1300°C, followed by the build-up of tensile stresses. The applied cyclic heating up and cooling down led to the repetitive formation of compressive and tensile stresses, with temperature dependencies oscillating with the number of applied laser pulses. The observed relatively high tensile stress level of ~1100 MPa in WC was a consequence of the stabilising function of the coating, which hindered the initiation of surface hot cracks and stress relaxation. The stress evolution was coupled with changes in XRD peak broadening, which however strongly depended on the particular *hkl* reflections and showed oscillatory behaviour within a single temperature cycle. In summary, the unique diffraction set-up revealed stress levels and provides insight into the WC-Co composite plastification mechanism governing the stress build-up and relaxation in locally thermo-shocked WC-Co inserts at millisecond time resolution.

Corresponding Author:

**Assoc.-Prof. Dr. Jozef Keckes*
Department of Materials Science
Montanuniversität Leoben
Jahnstrasse 12
A-8700 Leoben
Austria
Phone: +43 3842 804 303
Fax: +43 3842 804 116
E-mail: jozef.keckes@gmail.com

[a] *These authors contributed equally to this work.*

Keywords

synchrotron XRD,
hard metal,
laser heating,
thermal fatigue,
plasitfication,
stress evolution

I. Introduction

WC-Co hard metal cutting inserts are composite materials based on hard ceramic tungsten carbide and a cobalt metallic binder [1]. They are extensively used in the machining tool industry due to their high hardness and toughness as well as excellent wear and high-temperature characteristics. In order to increase the life-time of the inserts, ceramic coatings such as TiN, Al_2O_3, TiAlN and CrAlN with a thickness of several micrometres are usually deposited onto the hard metal by means of chemical (CVD) or physical (PVD) vapour deposition processes [1].

In metal cutting operations, the friction between insert and metal induces localised high temperature shocks on the cutting inserts with peak temperatures reaching more than 1000°C [2]. During cyclically interrupted cutting processes, such as milling, the tool lifetime is affected by millisecond temperature and mechanical pulses, which occur as a result of interrupted tool-workpiece contact and cause wear and thermal fatigue. The periodic localised thermal shocks cause rapid changes in lateral and depth-dependent stress distributions, as a result of (i) thermal stress changes caused by the mismatch of coefficients of thermal expansions (CTEs) between coating and substrate, (ii) intrinsic stress changes as a result of microstructural (and also phase) changes in the coating and (iii) non-uniform temperature distributions across the cutting insert [3]. Consequently, there exist several stages of cutting insert damage caused by the thermo-mechanical fatigue, as discussed by Kirchhoff et al. [2] involving the formation of surface and delamination cracks and coating spalling. Crack formation is fostered by the build-up of tensile residual stresses triggered by localised plastification of substrate [4] and coating [5]. For a particular coating-substrate system, the degree of damage depends on the maximum temperature and duration of applied pulses as well as on the magnitude of the friction-induced thermo-mechanical stress and the number of applied cycles.

The cyclic thermo-mechanical fatigue of WC-Co composites has been studied both experimentally [6, 7, 8] as well as using simulation tools to quantify thermal metal machining tool loads [9, 10]. In order to predict the degree of local damage induced by the interrupted tool-workpiece contact and wear, a variety of material parameters have to be taken into account, such as CTEs, thermal conductivities and elasto-plastic properties of the coating-substrate composite, all of which are dependent on temperature, crystallite size as well as geometry and the time-scale of the underlying process. Most recent experimental studies were devoted primarily to the ex-situ analysis of thermo-mechanically loaded inserts from real cutting experiments [2] and WC-Co composites treated in laser thermal shock experiments [7, 8, 11]. The latter provide the opportunity to evaluate the influence of controllably induced thermo-mechanical damage, separated from occurring friction loads. The ex-situ studies of the laser shocked samples manifested the complex nature of thermal fatigue resulting from the formation of lateral and depth gradients of stresses, microstructure and phases, as discussed by Bartosik *et al.* [11]. Although several studies have been performed on laser shock induced damage in coating-substrate composites, the underlying localised time and temperature-dependent evolution of phases, microstructure, and stresses as well as the incorporated mechanisms in terms of material science still remain unknown.

Recently, a novel in-situ characterisation approach based on a millisecond synchrotron X-ray diffraction (XRD) analysis coupled with a pulsed laser sample treatment was introduced by Kostov *et al.* [12]. The complex experimental set-up makes it possible to characterise temporal evolutions of lattice strain, stress and microstructure, as well as to perform real-time monitoring of phase transformations of rapidly heated samples in the laser focus of several millimetres, which overlaps with the synchrotron X-ray beam footprint on the investigated sample surface. Predominantly, this set-up was applied to investigate the laser surface hardening of steel [13].

In the current work, this well-established synchrotron X-ray set-up [12] was used to in-situ characterise WC-Co inserts coated with a PVD TiCN/Al_2O_3 bilayer, which was locally heated using a high-power diode laser (HPDL) up to a maximum temperature of 1300°C, applying (i) a single and (ii) five successive heating cycles. The objectives were (i) to test the transferability of the synchrotron XRD set-

up to the field of cutting inserts analysis, (ii) to evaluate the time-dependent evolution of stresses and finally the formation of residual stresses, the evolution of microstructure and (iii) to assess thermally driven mechanisms governing stress build-up and relaxation.

II. Experiment and Methodology

The medium grained WC-Co inserts studied in this work came in SNUN 120412 geometry (according to ISO 1832) with a chemical composition of 77 wt% WC, 12 wt% mixed carbides and 11 wt% Co. All inserts were mechanically fine-polished to minimise surface roughness and subsequently coated with a CVD bilayer architecture featuring a TiCN base layer with a thickness of ~6.5 µm and a top layer of α-Al_2O_3 with a thickness of ~3.5 µm. The TiCN base layer was deposited from precursors of TiCl-CH_3CN-H_2-N_2-CO at a temperature of 900°C and a pressure of 100 mbar, while the overlying α-Al_2O_3 top layer was grown using $AlCl_3$-CO_2-H_2-H_2S precursors at a temperature of 1000°C and a pressure of 75 mbar. The coating deposition was carried out in an industrial scale SuCoTec SCT600TH CVD plant. Subsequent to the deposition, the coated inserts were subjected to a wet blasting treatment with the central aim of changing the residual stress state of coating and substrate from tensile to compressive as summarised in our previous work [14].

The inserts were analysed using the dedicated in-situ XRD set-up described by Kostov et al. in [12] at the P05 beamline of the Petra III synchrotron source of DESY in Hamburg, Germany. Enhancements of the set-up were reported in [15, 16]. In the used experimental configuration (Fig. 1) the incident focussed X-ray beam with intensity I_o hit the laser heated cutting insert at an angle χ with respect to the sample normal. Diffracted intensities I^{hkl_1} and I^{hkl_2} from the two *hkl* Debye-Scherer rings were collected by the stripe detectors 1 to 4, positioned at four different orientations with respect to the sample normal. Each of the hkl_1 and hkl_2 reflections was recorded at two different diffraction vectors $N_i^{hkl_1}$ and $N_i^{hkl_2}$ at orientations ψ_i (i = 1, 2) and allowed the analysis of stresses according to the $\sin^2\psi$ method. The set-up featured a helium-filled process chamber with a sample stage and a HPDL unit LDM 4000-100 from Laserline GmbH, Mühlheim-Kärlich, Germany, with a maximum power of ~4 kW at a wavelength of 1020 nm. The laser beam possessed a Gaussian intensity distribution with a focus spot diameter of ~5.8 mm. The sample surface temperature and thereby the laser power output was controlled during laser shocks using a one-color pyrometer operating at a sampling rate of 100 Hz in the temperature range of 190–1500°C. The coated inserts were heated to a maximum temperature of 1300°C, applying a heating rate of 1000°C/s. The cooling phase was, in an analogous manner, realised by means of temperature control at a cooling rate of -1000°C/s down to a temperature of ~200°C or, finally to ambient temperature, *i.e.* the controlled cooling was achieved by adjusting the laser power. However, starting at a temperature of approx. 600°C the cooling rate was smaller, due to the relatively large sample volume and the non-zero heat capacity of the cutting inserts.

In the XRD experiment, a photon energy of 10.180 keV (λ = 0.12189 nm) was used, while the X-ray spot was set to dimensions of 1 × 1 mm^2 by use of a cross slit aperture. The diffraction signal from the samples was collected using four fast silicon strip line detectors Mythen 1K from Dectris Ltd., Switzerland, featuring a pitch size of 50 µm, of which the angular positions were calibrated using a LaB_6 powder standard. Throughout the in-situ experiments, the detector sampling rate was set to 20 Hz, resulting in an exposure time of 50 ms.

During all performed in-situ experiments, the four detectors recorded the diffraction signal from multiple different {*hkl*} crystallographic planes with four distinct orientations with respect to the sample normal (Fig. 1). Due to the weak diffraction signal from the coatings, it was, unfortunately, not possible to evaluate the diffraction data from the Al_2O_3 and TiCN coating sublayers and the measurements provided sufficient diffraction information from the WC phase only. At a heating rate of 1000°C/s and the applied sampling time of 50 ms, the resulting temperature resolution was ~50°C. In the temperature range of 25–1300°C, it was possible to collect *hkl* diffraction peaks at diffraction angle positions $2\theta_{\psi_i}^{hkl,T}$, using

each of the two detector pairs, where ψ_i represents the angle between the diffraction vector and the sample normal (Fig. 1). The detector pairs were mounted in such a fashion, that detectors 1 and 2 covered a 2θ-range of 140–158°, while detectors 3 and 4 covered the range of 121.5–133°. The recorded diffraction peaks were fitted using a Pseudo-Voigt function, followed by the evaluation of integral breadths $\beta_{\psi_i}^{hkl,T}$ and positions of Bragg's angle $\theta_{\psi_i}^{hkl,T}$ of the peaks. The diffraction data were then used to quantify lattice spacings $d_{\psi_i}^{hkl,T}$ according to Bragg's law. Subsequently, $\theta_{\psi_i}^{hkl,T}$ versus ψ_i, dependencies were used to evaluate in-plane X-ray elastic strains $\varepsilon_{el}^{hkl,T}$ and thermal strains $\varepsilon_{th}^{hkl,T}$ by considering the strain free direction $\psi^{hkl,*}$, which can be calculated based on the assumption of an equi-biaxial stress state and a negligible out-of-plane stress component in the WC phase as $\psi^{hkl,*} = -2s_1^{hkl}/s_2^{hkl}$. In-plane X-ray elastic strains were used to quantify magnitudes of in-plane stress using $\sigma^{hkl,T} = \varepsilon_{\mathrm{el}}^{hkl,T}/s_2^{hkl}$. Parameters s_1^{hkl} and s_2^{hkl} represent X-ray elastic constants calculated for WC based on the Kröner grain interaction model [17] using WC single crystal elastic constants c_{11} = 7.2 × 10^{11} Pa, c_{12} = 2.54 × 10^{11} Pa, c_{33} = 9.72 × 10^{11} Pa and c_{44} = 3.28 × 10^{11} Pa [18]. Further details on the evaluation procedure can be found elsewhere [12].

In an entirely isotropic case, the evaluated in-plane stresses $\sigma^{hkl,T}$ would be independent of *hkl*, assuming that the applied grain interaction model is valid. It often occurs, however, that in the case of neutron and synchrotron diffraction analyses of stresses, the evaluation procedure results in strongly *hkl*-dependent values of $\sigma^{hkl,T}$. This effect can have various origins, such as the anisotropic elastic stiffness of individual diffracting grains, grain-size dependent plasticity, intragranular strains, anisotropic strain relaxation along specific slip systems *etc*. Therefore, it is convenient to introduce a weighted or average $\sigma^{\mathrm{avg},T}$, which is determined as a mean value from the evaluated $\sigma^{hkl,T}$ with a texture index of 1 [19].

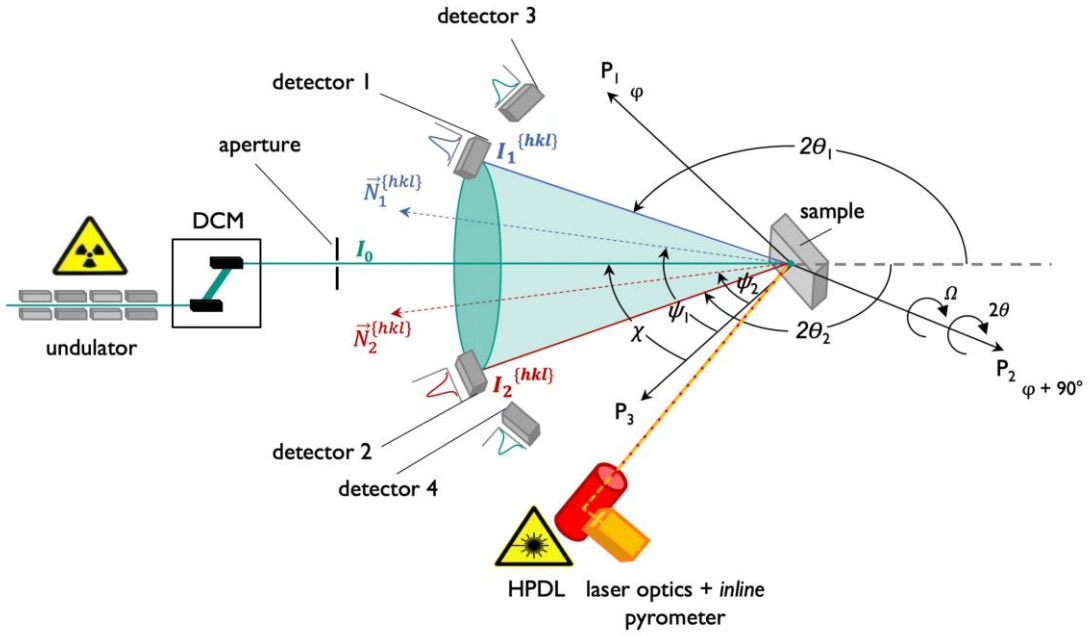

Figure 1. Schematic drawing of the experimental set-up at the P05 beamline of PETRA III at DESY showing the geometrical arrangement of sample, X-ray beam, HPDL, pyrometer and the four detectors. The set-up was installed in a process chamber, which guaranteed laser radiation protection and application of a defined atmosphere for the temperature controlled process (see also [12])

III. Results and Discussion

III.A. SEM Analysis

The surfaces and cross-sections of the irradiated cutting inserts were analysed ex-situ using optical microscopy and scanning electron microscopy (SEM) after the laser shock experiments. Low-magnification surface (a) and cross-sectional (b) optical micrographs of the sample heated up for five cycles using the laser set-up are presented in Fig. 2, together with a secondary electron SEM cross-section (c) prepared by focussed ion beam milling. Neither the optical, nor the SEM analysis indicated apparent structural sample damage induced by thermal fatigue.

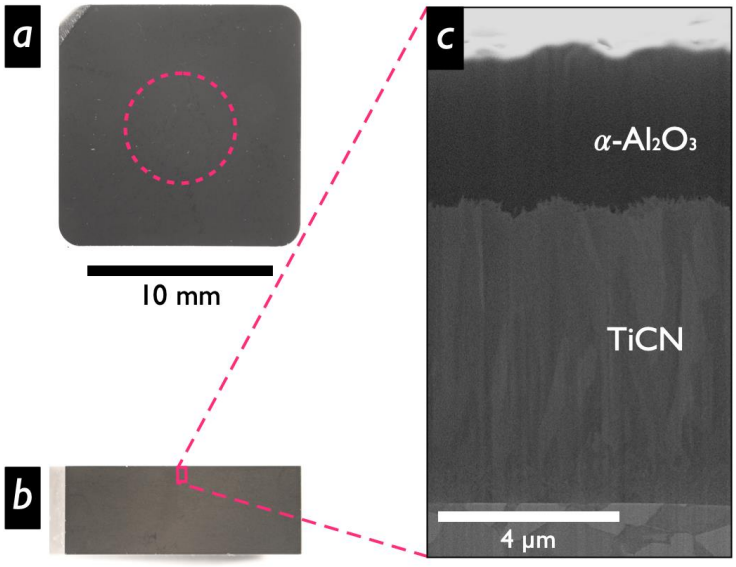

Figure 2. Optical (a, b) and secondary electron SEM (c) micrographs from the cutting insert surface (a) with indication of the area irradiated by the laser beam and cross-sections (b, c) of the WC-Co/TiCN/Al_2O_3 sample, which indicated no structural sample damage after applying five successive laser pulses.

III.B. Single Laser Pulse Experiment

In the first conducted experiment, the HPDL unit from Fig. 1 was used to heat a WC-Co/TiCN/Al_2O_3 sample to a surface temperature of 1300°C, which was reached within ~1.1 s, followed by a controlled cooling down phase to a surface temperature below ~200°C within a time span of ~2.2 s. In Fig. 3, examples of XRD patterns from two of the detectors indicate the relative shifts of WC 114 and 312 reflections due to the presence of stress in the probed WC volume, as well as the shifts of the individual reflections caused by the temperature changes. Furthermore, the selected diffractograms from detectors 1 and 2 indicate that the peak widths of the individual diffraction lines change during processing, indicating changes in the local microstructure through the laser irradiation.

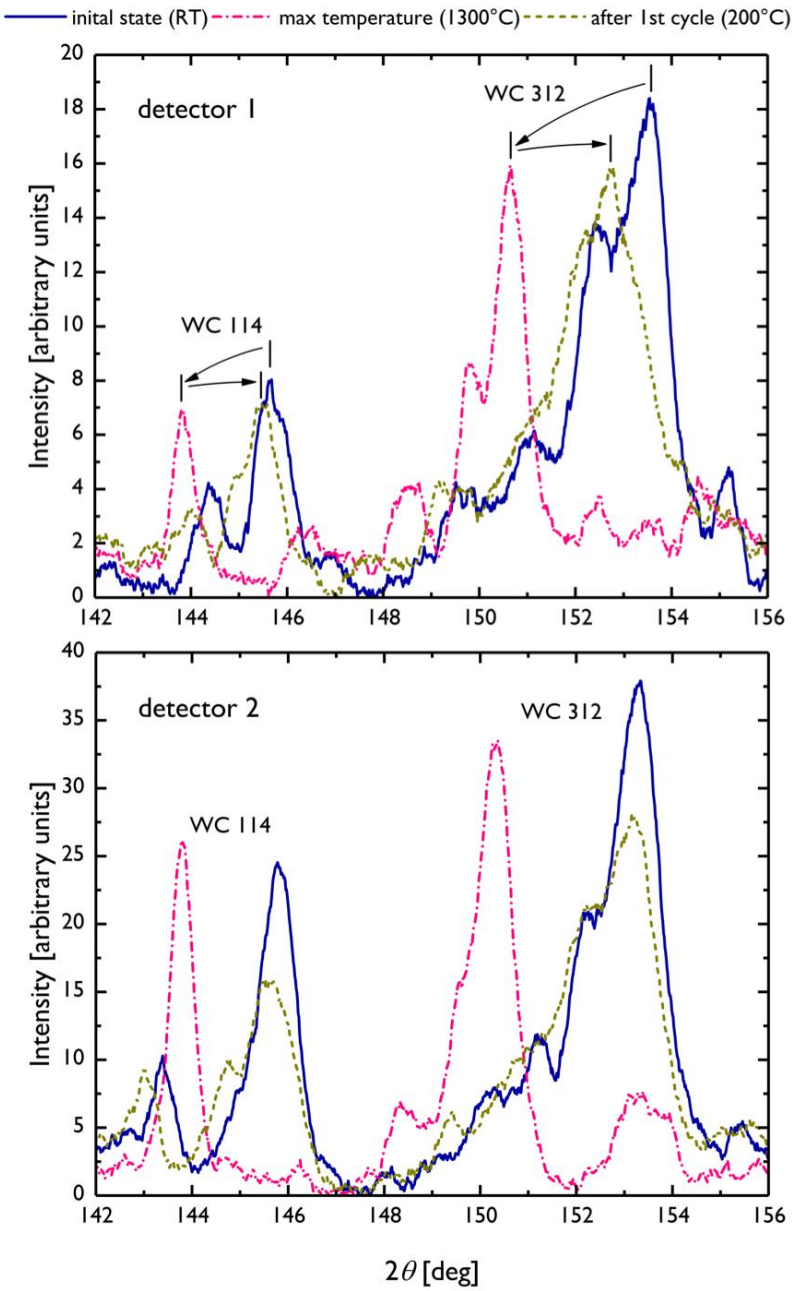

Figure 3. Examples of XRD patterns recorded by detectors 1 and 2, mounted at two different angular orientations ψ_i with respect to the sample normal. The relative shifts in WC phase reflections recorded during one applied laser pulse at room temperature (RT), 1300°C and 200°C are the result of lattice parameter thermal expansion and the presence of stresses in the imprint of the X-ray beam on the sample surface. Unfortunately, the diffraction signal from the Al_2O_3 and TiCN phases was too weak to be further analysed.

High temperature XRD (HT-XRD) data, recorded by detectors 1 and 2 during the temperature cycle, are presented together with temperature data from the pyrometer in Fig. 4 as a function of the processing time in a 2D contour plot. After initiating the laser heating, the sample surface reached a temperature of 200°C, which was the approximate sensitivity threshold of the pyrometer. Further heating resulted in a shift of WC diffraction peaks towards lower 2θ angles on all four detectors, as a consequence of WC thermal expansion and the related build-up of mechanical stresses. Diffraction peaks shifted back towards larger 2θ values during the temperature decrease in the subsequent controlled cooling down phase.

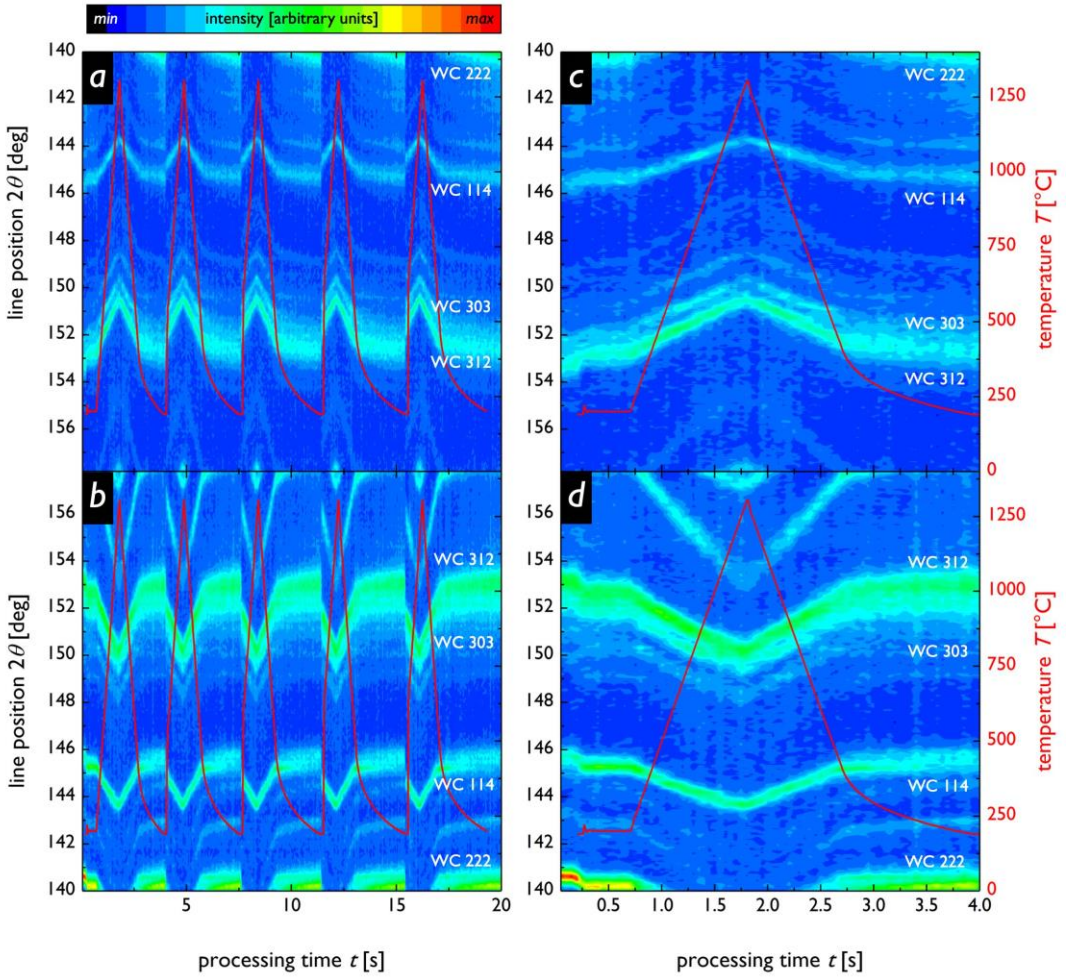

Figure 4. Examples of HT-XRD patterns (2D contour plot) recorded by detectors 1 (a, c) and 2 (b, d) revealed shifts of WC reflections during five successively applied laser pulses (a, b), as well as during the first pulse (c, d) with a maximum temperature of ~1300°C measured by the pyrometer. The shifts of the reflections were caused by the thermal expansion of WC and the related formation of stresses. The pyrometer employed in recording the sample surface temperature was calibrated for a *T* range of 190–1500°C.

The recorded high-temperature data from the four detectors were subsequently used to evaluate thermal strains $\varepsilon_{\mathrm{th}}^{hkl,T}$. The time dependencies of $\varepsilon_{\mathrm{th}}^{hkl,T}(t)$ presented in Fig. 5 show the increase and decrease of thermal strains during the single laser pulse experiment. Data of $\varepsilon_{\mathrm{th}}^{hkl,T}(t)$ can be correlated with the temperature changes while all dependencies $\varepsilon_{\mathrm{th}}^{hkl,T}(t)$, *i.e.* for the 114, 303 and 312 diffraction lines of WC, show a very similar behaviour (cf. Fig. 5).

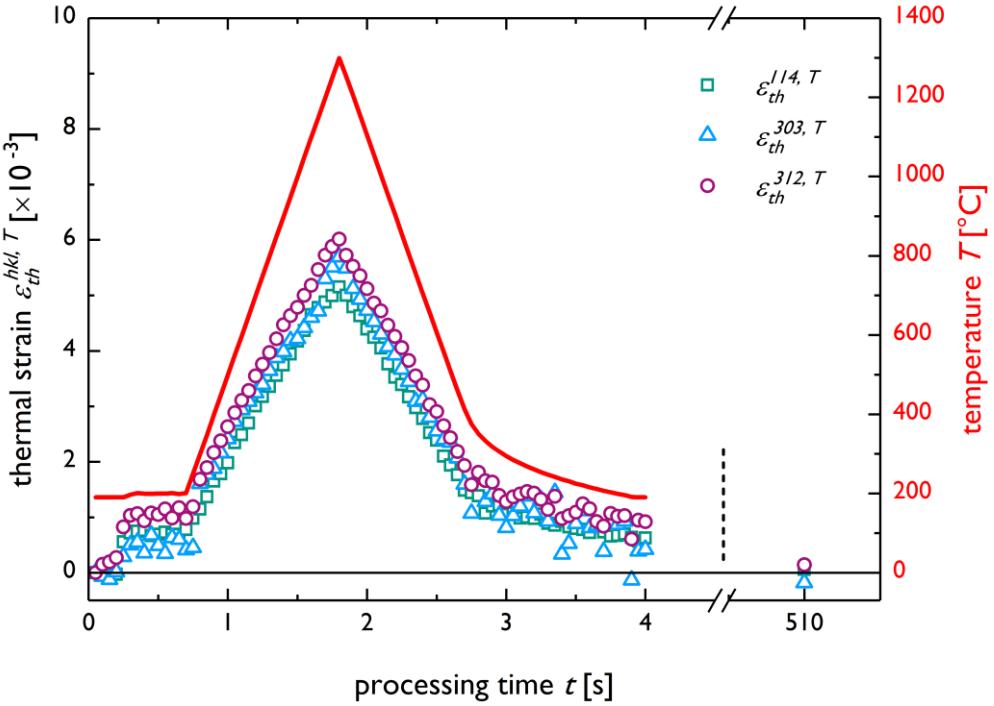

Figure 5. Time-dependent evolution of in-plane thermal strains $\varepsilon_{\mathrm{th}}^{hkl,T}(t)$ for selected WC *hkl* reflections. The pyrometer employed in recording the sample surface temperature was calibrated for a *T* range of [190–1500°C].

As indicated in Section 2, high-temperature diffraction data were used to evaluate the temperature-dependent evolution of in-plane stresses in the laser heated sample volume. In Fig. 6, temperature dependencies of *hkl*-dependent in-plane stress $\sigma^{hkl,T}$ for three representative reflections are presented together with the average in-plane stress profile $\sigma^{\mathrm{avg},T}$. It is apparent that all $\sigma^{hkl,T}$ dependencies show similar qualitative behaviour, *i.e.* an increase in compressive stress and subsequent formation of radial tensile stresses, as discussed in our previous reports [3–20]. In the data, one can identify (i) varying maximum magnitudes of individual $\sigma^{hkl,T}$ dependencies (occurring in both domains, tensile and compressive alike) as well as (ii) slightly different shapes of the dependencies $\sigma^{hkl,T}(t)$.

The observation of *hkl*-dependent in-plane stresses can, in general, be interpreted by the (*hkl*)-dependent elasto-plastic anisotropy of hexagonal WC [21], which influences the WC deformation in both the elastic and plastic domains. Therefore, it is not trivial to obtain a continuum mechanics equivalent of elastic strains and stresses from the performed synchrotron X-ray diffraction measurements. The evaluated values of averaged in-plane stress $\sigma^{\mathrm{avg},T}$, however, provide a reasonable representation of the temperature and time-dependent evolution of in-plane stresses within the sample (Fig. 6). Preceding the laser pulse experiment, the value of $\sigma^{\mathrm{avg},T}$ is ~-300 MPa. During the heating up to T ~750°C, $\sigma^{\mathrm{avg},T}$ increased in the compressive domain to a value of ~-1300 MPa due to the thermal expansion of the laser irradiated WC-Co substrate volume and the constraint given by the colder surrounding material. Exceeding measured sample surface temperatures of ~750°C at t ~1.2 s led to plastification effects in the WC-Co composite, resulting in compressive stress relaxation. At the maximum applied temperature of ~1300°C, $\sigma^{\mathrm{avg},T}$ relaxed to ~-450 MPa. Subsequent controlled cooling down led to a further decrease of the compressive stress components, with $\sigma^{\mathrm{avg},T}$ reaching the zero level at a temperature slightly above ~1000°C. Further cooling down initiated the build-up of average tensile stresses of up to ~1100 MPa, most probably as a consequence of the radial enlargement of the plastically deformed material in the centre of the laser focus. After the controlled cooling phase, tensile stresses relaxed to a plateau level of ~400 MPa within ~500 s as the temperature of the cutting insert converged to ambient temperature. A

local minimum in $\sigma^{avg,T}$ occurring at t ~1.7 s coincided with the PVD coating deposition temperature and could be the consequence of coating-substrate interaction. In the experiments the pyrometer-based temperature measurement was calibrated for a T range of 190–1500°C, i.e. values presented in Figs. 4–8 below a threshold of 190°C at T = 0 to ~0.75 s did not reflect the true sample surface temperature. The measured temperature values reflected the temperature at the coating surface, while the heat transfer from the coating to the surface-near substrate region was assumed to take place quasi-instantaneously.

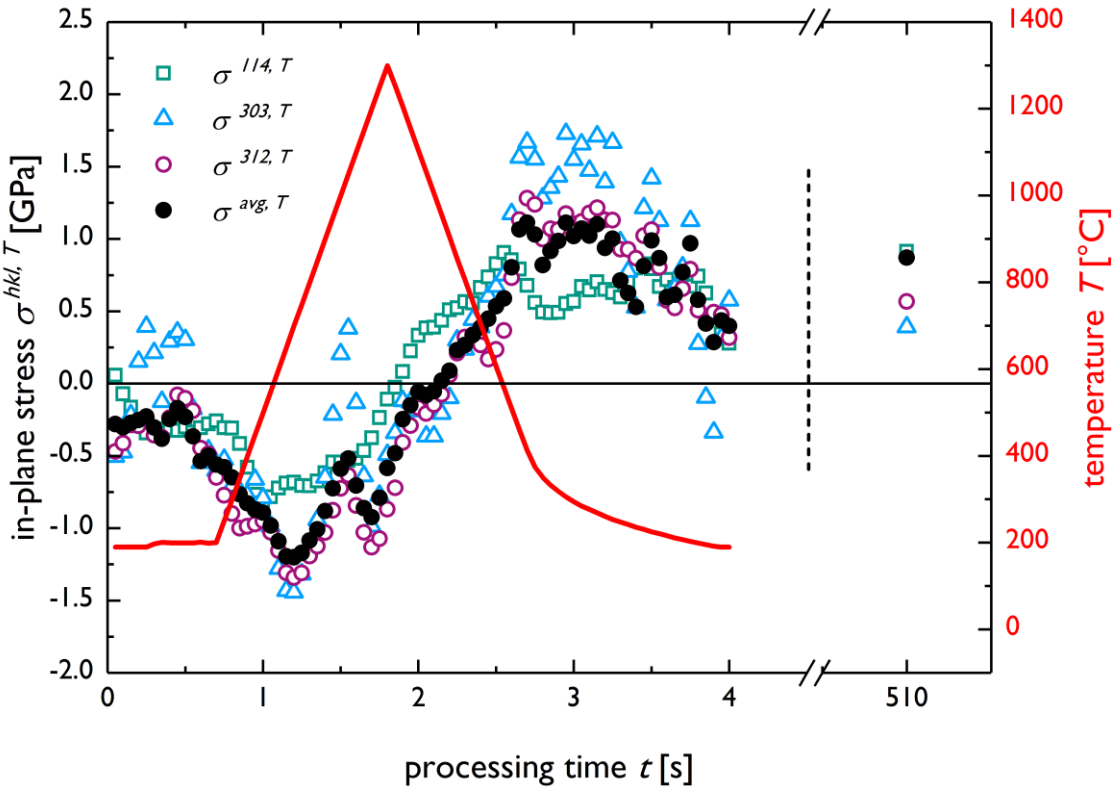

Figure 6. Time-dependent evolutions of in-plane stresses $\sigma^{hkl,T}(t)$ for selected WC *hkl* reflections and averaged in-plane stress $\sigma^{avg,T}$ during one single laser pulse. Individual profiles of $\sigma^{hkl,T}$ differed significantly between particular *hkl* reflections. The pyrometer employed in recording the sample surface temperature was calibrated for a T range of [190–1500°C].

The individual diffractograms used to depict the time and temperature evolution of individual *hkl* reflections in Fig. 4 were fitted using a Pseudo-Voigt function. Values of integral breadths $\beta^{hkl,T}$ for selected reflections are presented in Fig. 7. Since the values of $\beta^{hkl,T}$ differed between individual reflections, data of $\beta^{hkl,T}$ presented in Figs. 7 and 8 have been normalised using the value of $\beta^{hkl,T}$ obtained at room temperature before the experiment, as a reference. Remarkably, the observed profiles of $\beta^{hkl,T}$ showed a periodic temperature evolution, *i.e.* all values of $\beta^{hkl,T}$ decrease during heating up, succeeded by the appearance of a local maximum at the peak temperature of ~1300°C, after which $\beta^{hkl,T}$ values started to rise again before saturating (cf. Fig. 7). In the main, the integral breadth of XRD peaks correlated with the size of coherently diffracting domains $\langle D \rangle$, as well as structural crystallographic defects such as dislocations and various other crystal lattice distortions, represented by inhomogeneous, i.e. non-directional, strains of 2nd and 3rd order [22]. In addition, $\langle D \rangle$ also correlates with the intrinsic

contribution of the diffraction system, which is referred to as instrumental broadening. Since, in the present case, changes in $\langle D \rangle$ of the ceramic material can be supposedly neglected (at temperatures significantly smaller than the WC melting point temperature of ~2870°C), the periodic integral breadth profiles in Fig. 7 can be interpreted by reversible annihilation and formation of structural defects in WC crystallites [20]. It is supposed that a certain type of structural recovery (cf. Sec. IV) occurs in the WC-Co composite material during heating up, and that during the cooling down phase, new defects are generated as a result of the formation of stresses in the laser irradiated sample volume. The appearance of the observed local maximum at ~1300°C and possible governing mechanisms are discussed in Section IV.

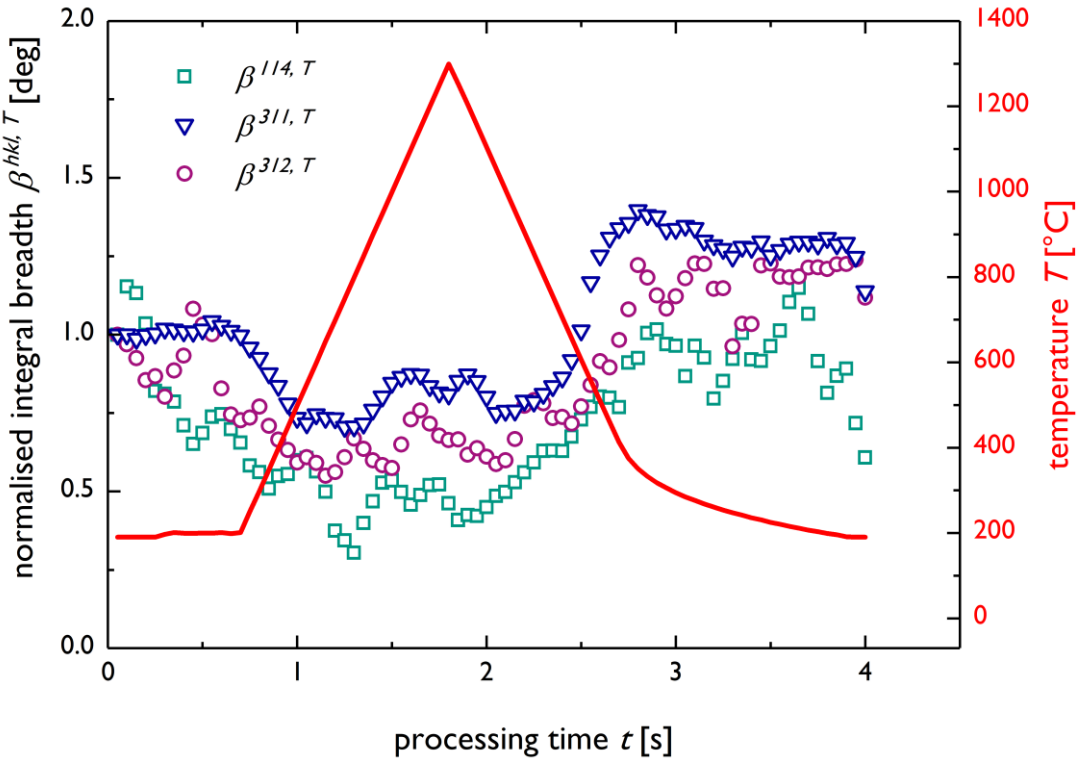

Figure 7. Time-dependent evolution of normalised integral breadths $\beta^{hkl,T}(t)$ for selected WC *hkl* reflections during one single laser pulse, indicating oscillatory peak broadening behaviour. The absolute changes in $\beta^{hkl,T}$ values differ significantly between the individual *hkl* reflections.

III.A. Multiple Laser Shot Experiment

A follow-up in-situ experiment including five successive laser pulses in the temperature range of 25 to 1300°C was performed in order to evaluate the effect of multiple heating up and cooling down cycles on the evolutions of $\sigma^{\text{avg},T}(t)$ and $\beta^{hkl,T}(t)$, which are presented together in Fig. 8. The temperature dependencies of $\beta^{hkl,T}$ (Fig. 8a) indicate similar behaviour as in the case of the single pulse experiment (cf. Fig. 7), *i.e.* inverse temperature dependence with pulse-number independent minimum $\beta^{hkl,T}$ values occurring at the peak temperatures of 1300°C for all five successive reflections and pulses.

Also, in the case of averaged in-plane stress $\sigma^{\text{avg},T}$ presented in Fig. 8b, c, the $\sigma^{\text{avg},T}(t)$ profile shows a behaviour similar to that from the single pulse experiment (cf. Fig. 6). The data reveal that the in-plane stresses turn compressive after the initiation of each heating pulse, and become tensile during the successive cooling down phase. In a similar fashion as in Fig. 6, the maximum compressive stress was not observed at the peak temperature, but was reached at a time lag a few hundred degrees below. At the applied maximum substrate temperature, stresses were still in the tensile regime before reaching the zero level during cooling down at about ~1000°C. Furthermore, the time-dependent behaviour of

$\sigma^{\mathrm{avg},T}(t)$ during five successive laser pulses shows the following attributes: (i) the maximum compressive stress during heating up of every pulse decreased with the number of applied laser pulses, while in a similar fashion (ii) the maximum magnitude of tensile stress of individual pulses was found to increase, before saturating. In the aftermath of the final pulse, the tensile stress level started to decrease exponentially and tended to saturate at a level of ~400 MPa. This stress relaxation process appeared to continue until the insert reached ambient temperature (Fig. 8). Additionally, the detailed data in Fig. 8c, collected during the first heating cycle, indicated that the relaxations of compressive and tensile stresses start at ~650°C and 350°C, respectively.

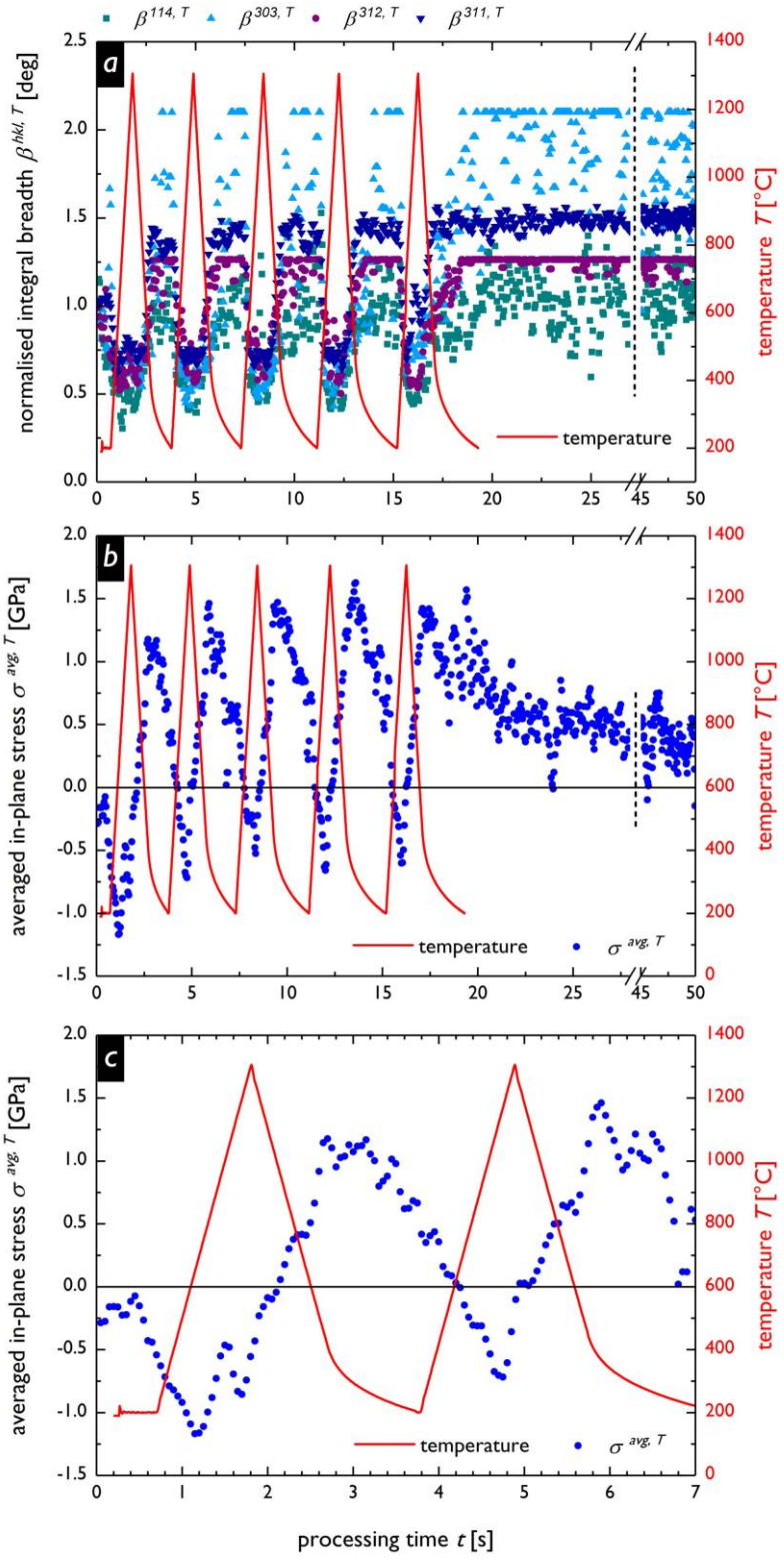

Figure 8. Time-dependent evolution of normalised integral breadth $\beta^{hkl,T}(t)$ (a) and averaged in-plane stress $\sigma^{\mathrm{avg},T}$ (b) during five successively applied laser pulses correlated with the corresponding substrate temperature. Detailed plot of $\sigma^{\mathrm{avg},T}$ for the first two applied pulses (c). The pyrometer used for recording the sample surface temperature was calibrated for a T range of 190–1500°C.

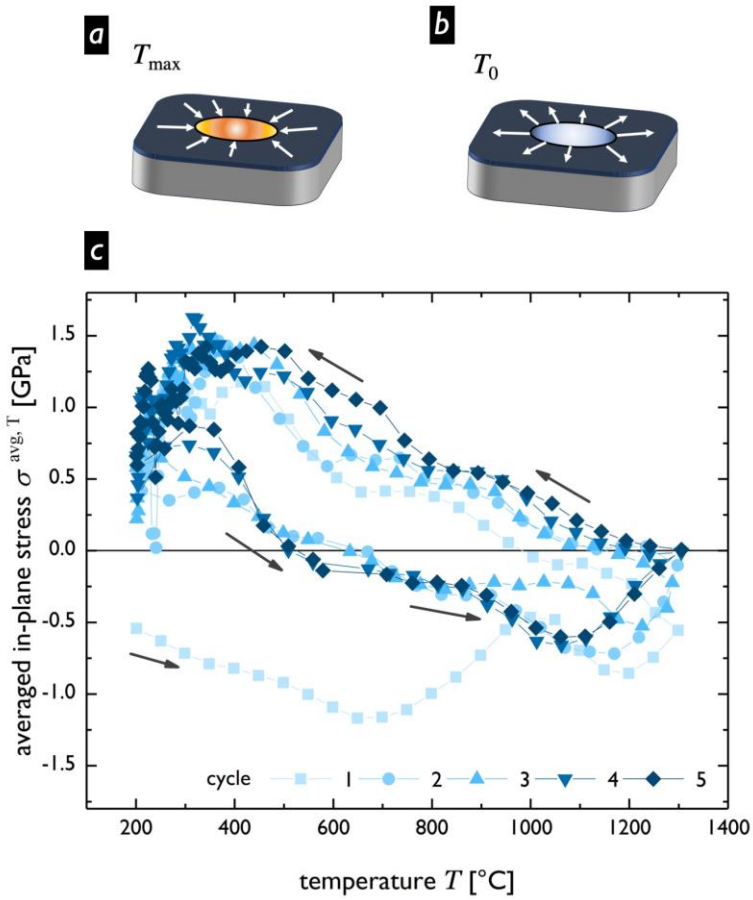

Figure 9. Schematic depiction of compressive (a) and tensile (b) stress formation in the material in and surrounding the laser irradiated spot in the investigated cutting inserts during heating up and cooling down, respectively. In (c), experimental data from Fig. 8c shows the time evolution of averaged in-plane stress $\sigma^{\mathrm{avg},T}$ as a function of the measured sample temperature during five successive laser pulses. It reveals the realisation of a cycle-dependent quasi-steady state after a transient phase during the first laser pulse.

IV. Discussion on Governing Mechanism

In-situ synchrotron X-ray diffraction studies of coated WC-Co cutting inserts during laser processing revealed insight into strain, stress, and microstructure evolution in real time. Time resolved lattice strain and broadening of diffraction profiles can be used for the assessment of deformation and degradation mechanisms (cf. results presented in Figs. 6, 7, and 8).

The mechanisms of compressive and tensile stress formation during heating up and cooling down are schematically depicted in Figs. 9a and 9b, respectively. The substrate heating up effects the rapid thermal

expansion of the irradiated WC-Co volume, which is itself constrained by the cooler surrounding material, therefore resulting in the build-up of compressive stresses up to a level of the WC-Co composite's limit of plastic deformation. During the subsequent cooling phase, the plastically deformed material in the laser heated spot contracted but was constrained by the surrounding material which led to the development of tensile stresses.

Based on the lattice strain determined for various $\{hkl\}$ lattice planes, averaged stress values $\sigma^{\mathrm{avg},T}$ were calculated following the approach proposed by Daymond [19] (cf. Figs. 6 and 8). The average stress distributions show that the maximum compressive stress of -1300 MPa was reached in the laser heated spot at a temperature of ~750°C during the first heating cycle, while further heating up led to the relaxation of compressive stresses, with total relaxation reached during the cooling down process, with $\sigma^{\mathrm{avg},1000°\mathrm{C}} \cong 0$. The observed decrease in stress during heating up at temperatures above ~750°C (Figs. 6 and 8b,c) can be correlated with the oscillatory behaviour of $\beta^{hkl,T}$ (Fig. 7), where values decreased, increased, and again decreased during one temperature pulse. In order to understand this unexpected behaviour, it must be considered that the yield stress $R_{\mathrm{p}\,0.2}$ of WC-Co composites of ~3500–7000 MPa at room temperature [4, 23] decreased rapidly by a factor of about five between 25°C and 900°C [24]. Above a temperature of 700°C, the yield strength was observed to decrease even more rapidly than at lower temperatures [24]. Also, pure WC was reported to show relatively ductile behaviour with a tensile fracture strain under bending conditions of larger than 0.2 % at 1000°C [21]. Therefore, the start of the compressive stress relaxation observed at stress levels of $\sigma^{\mathrm{avg},750°\mathrm{C}} \cong -1300$ MPa (cf. Figs. 6, 8c) as well as the increase in $\beta^{hkl,T}$ (Fig. 7) during heating up at ~750°C can be correlated with the onset of plastification of the WC crystallites. Additionally, it must be expected that the heating up also resulted in plastification and softening of the Co binder phase, of which the temperature evolution remained inaccessible. Therefore, it can be generally supposed that the decrease in compressive stress at ~750°C in Figs. 6 and 8 can be attributed to the softening of the interacting WC and Co phases within the hard metal composite.

Further heating to temperatures above 750°C most probably induces increased softening of the WC-Co composite accompanied by the stress relaxation in WC, and supposedly also Co, and the formation of microstructural defects like dislocations, slip planes and grain boundaries [21], which are responsible for the occurrence of the observed local maximum of $\beta^{hkl,T}$ in Fig. 7. During the second (and later) pulses, the onset of WC-Co composite plastification points appeared to occur at higher temperatures, as can be observed in detail in Fig. 8c.

The interesting effects of (i) the increasing maximum magnitude of tensile stresses $\sigma^{\mathrm{avg},T}$ in Fig. 8b,c with the increasing number of applied pulses and (ii) the shift of the stress relaxation temperature (Fig. 8c) already after the first heating cycle can be attributed to the pulse-number related (stepwise) hardening of the WC phase. The controlled cooling down resulted in the build-up of a three-dimensional tensile stress distribution, possessing a two-dimensional Gaussian lateral profile, which decreased exponentially as a function of sample depth [11, 20, 25, 26]. The presence of the coating protected the WC-Co substrate from (i) heat transfer into the substrate volume and (ii) the formation of hot cracks, as documented for CrN coated steel [26]. This behaviour was obviously indirectly observed also in the present case, where the cooling down after the laser pulses resulted in the formation of tensile stresses, with stepwise increasing amplitudes. Literature values of tensile strength of WC skeletons produced by removing the binder phase by etching, are in the range of ~500 MPa, and are most likely influenced by the presence of etching-induced microvoids [21]. However, measured maximum tensile stresses $\sigma^{\mathrm{avg},T}$ in the WC phase showed values of up to ~1100 MPa. This observed relatively high tensile strength of the investigated substrate-coating composite structures is attributed to the protective effect of the coating, which hinders the initiation of hot cracks at the surface of the WC-Co cutting insert, as demonstrated by Kirchlechner *et al.* [20], which is of relevance when considering the application of hard metals e.g. in metalworking operations. A similar effect was observed ex-situ in the case of CrN-coated

steel. A further effect apparent in Fig. 8b, is the stepwise decrease of the maximum compressive stress values with the increasing number of applied pulses. This observation can be interpreted by the cyclic sample heating, reducing the lateral temperature gradient and subsequently also the compressive thermal stresses imposed on the irradiated spot by the surrounding material.

Furthermore, it is interesting to observe that the values of integral breadth belonging to individual *hkl* reflections are differently affected by the rapid local temperature changes within the sample. During heating up from 25 to 1300°C, $\beta^{311,T}$ decreased only by ~25%, while $\beta^{114,T}$ changes by ~80% (Fig. 7). The unequal changes in the broadening of the WC *hkl* reflections indicated anisotropic plastic deformation within the WC hexagonal crystal accompanied by anisotropic annihilation and formation of structural defects. As discussed by Österberg *et al.* [21], there exist several plastic deformation mechanisms in hexagonal WC crystal, including plastic deformation by dislocation climb, glide and WC/WC grain boundary sliding. Transmission electron microscopy studies on plastically deformed samples confirmed that WC plastic deformation is a highly anisotropic process, occurring only along a limited number of families of crystallographic planes [21, 27]. Hence, the observed differences in the evolutions of $\beta^{hkl,T}$ in Fig. 7 between various reflections can be interpreted referring to this anisotropic property of WC. It is supposed that the laser pulses resulted in the formation of tensile and compressive stresses in the WC phase, which are partly relaxed by particular slip mechanisms [21].

The development of $\sigma^{\mathrm{avg},T}$ as a function of measured sample temperature is presented in Fig. 9c. The data show the transient behaviour of $\sigma^{\mathrm{avg},T}$ during the heating up phase of the first applied laser pulse, starting in the compressive domain. For the successive pulses, a quasi-steady state of the hysteresis loops arises, with minor shifts of $\sigma^{\mathrm{avg},T}$ towards higher tensile stress values for every pulse during cooling down, while during the heating up phase a shift of the cycle-dependent profiles of $\sigma^{\mathrm{avg},T}$ is not apparent.

V. Conclusions and Outlook

Time-dependent data of in-plane strains and stresses collected during in-situ laser pulse experiments indicated the formation of compressive and tensile stresses at 50 ms time resolution within the laser pulsed spot, with magnitudes decreasing and increasing with the number of applied pulses, respectively. Importantly, the in-situ stress and peak broadening values (Figs. 6-8) indicate the onset of plastic deformation of both the Co and the WC phase at temperatures above ~750°C, occurring during every applied heating cycle.

Methodologically, the synchrotron diffraction set-up allowed the study of the complex stress build-up and relaxation in coated locally thermo-shocked WC-Co inserts at millisecond time resolution and revealed anisotropic microstructural processes accompanying reversible microstructural transition mechanisms.

Acknowledgements

The authors gratefully acknowledge the financial support under the scope of the COMET program within the K2 Center “Integrated Computational Material, Process and Product Engineering (IC-MPPE)” (Project No 859480). This program is supported by the Austrian Federal Ministries for Transport, Innovation and Technology (BMVIT) and for Digital and Economic Affairs (BMDW), represented by the Austrian research funding association (FFG), and the federal states of Styria, Upper Austria and Tyrol.

References

[1] V. Sarin, Comprehensive Hard Materials, Elsevier, 2014.

[2] G. Kirchhoff, T. Göbel, H.-A. Bahr, H. Balke, K. Wetzig, K. Bartsch, Damage analysis for thermally cycled (Ti,Al)N coatings—estimation of strength and interface fracture toughness, Surf. Coatings Technol. 179 (2004) 39–46.

[3] M. Bartosik, R. Daniel, Z. Zhang, M. Deluca, W. Ecker, M. Stefenelli, M. Klaus, C. Genzel, C. Mitterer, J. Keckes, Lateral gradients of phases, residual stress and hardness in a laser heated Ti0.52Al0.48N coating on hard metal, Surf. Coatings Technol. 206 (2012) 4502–4510.

[4] T. Teppernegg, T. Klünsner, P. Angerer, C. Tritremmel, R. Ebner, C. Czettl, J. Keckes, R. Pippan, Residual stress and damage in coated hard metal milling inserts, Adv. Tungsten, Refract. Hardmaterials IX - Proc. 9th Int. Conf. Tungsten, Refract. Hardmaterials, 2014.

[5] T. Teppernegg, P. Angerer, T. Klünsner, C. Tritremmel, C. Czettl, Evolution of residual stress in Ti–Al–Ta–N coatings on hard metal milling inserts, Int. J. Refract. Met. Hard Mater. 52 (2015) 171–175.

[6] E.A. Álvarez, J.L. García, C.J.R. González Oliver, Thermal Cycling Behavior of Thin WC-Co Sintered Pellets, Adv. Eng. Mater. 19 (2017) 1600544.

[7] A. Kasterov, A. Shugurov, M. Kazachenok, A. Panin, C.-H. Cheng, I.-L. Chang, The effect of laser treatment of WC-Co coatings on their failure under thermal cycling, AIP Conf. Proc., AIP Publishing LLC, (2016) 020083.

[8] C. Peng, Y. Meng, W. Guo, Influence of Laser Shock Processing on WC–Co Hardmetal, Mater. Manuf. Process. 31 (2016) 794–801.

[9] A.W. Nemetz, W. Daves, T. Klünsner, W. Ecker, T. Teppernegg, C. Czettl, I. Krajinović, FE temperature- and residual stress prediction in milling inserts and correlation with experimentally observed damage mechanisms, J. Mater. Process. Technol. 256 (2018) 98–108.

[10] A.W. Nemetz, W. Daves, T. Klünsner, W. Ecker, J. Schäfer, C. Czettl, T. Antretter, Cyclic heat-up and damage-relevant substrate plastification of single- and bilayer coated milling inserts evaluated numerically, Surf. Coatings Technol. 360 (2019) 39–49.

[11] M. Bartosik, R. Daniel, Z. Zhang, M. Deluca, W. Ecker, M. Stefenelli, M. Klaus, C. Genzel, C. Mitterer, J. Keckes, Lateral gradients of phases, residual stress and hardness in a laser heated $Ti_{0.52}Al_{0.48}N$ coating on hard metal, Surf. Coatings Technol. 206 (2012) 4502–4510.

[12] V. Kostov, J. Gibmeier, F. Wilde, P. Staron, R. Rössler, A. Wanner, Fast *in situ* phase and stress analysis during laser surface treatment: A synchrotron x-ray diffraction approach, Rev. Sci. Instrum. 83 (2012) 115101.

[13] V. Kostov, Untersuchungen zur zeitaufgelösten Spannungsentwicklung und Eigenspannungsentstehung beim Laserstrahlstandhärten am Beispiel des Stahls 42CrMo4, (2014), PHD thesis, Karlsruhe Institute of Technology

[14] M. Tkadletz, J. Keckes, N. Schalk, I. Krajinovic, M. Burghammer, C. Czettl, C. Mitterer, Residual stress gradients in α-Al_2O_3 hard coatings determined by pencil-beam X-ray nanodiffraction: The influence of blasting media, Surf. Coatings Technol. 262 (2015) 134–140.

[15] D. Kiefer, J. Gibmeier, F. Beckmann, F. Wilde, In-situ Monitoring of Laser Surface Line Hardening by Means of Synchrotron X-Ray Diffraction, Mater. Res. Proc., Materials Research Forum LLC, (2017) 467–472.

[16] D. Kiefer, J. Gibmeier, F. Beckmann, Fast Temporal and Spatial Resolved Stress Analysis at Laser Surface Line Hardening of Steel AISI 4140, Mater. Res. Proc., Materials Research Forum LLC, (2018) 91–96.

[17] E. Kröner, Berechnung der elastischen Konstanten des Vielkristalls aus den Konstanten des Einkristalls, Zeitschrift für Phys. 151 (1958) 504–518.

[18] M. Lee, R.S. Gilmore, Single crystal elastic constants of tungsten monocarbide, J. Mater. Sci. 17 (1982) 2657–2660.

[19] M.R. Daymond, The determination of a continuum mechanics equivalent elastic strain from the analysis of multiple diffraction peaks, J. Appl. Phys. 96 (2004) 4263–4272.

[20] C. Kirchlechner, K.J. Martinschitz, R. Daniel, C. Mitterer, J. Donges, A. Rothkirch, M. Klaus, C. Genzel, J. Keckes, X-ray diffraction analysis of three-dimensional residual stress fields reveals origins of thermal fatigue in uncoated and coated steel, Scr. Mater. 62 (2010) 774–777.

[21] G. Östberg, K. Buss, M. Christensen, S. Norgren, H.-O. Andrén, D. Mari, G. Wahnström, I. Reineck, Mechanisms of plastic deformation of WC–Co and Ti(C, N)–WC–Co, Int. J. Refract. Met. Hard Mater. 24 (2006) 135–144.

[22] E. Mittemeijer, U. Welzel, The "state of the art" of the diffraction analysis of crystallite size and lattice strain, Z. Kristallog. 223 (9) (2008) 552–560.

[23] T. Klünsner, S. Marsoner, R. Ebner, R. Pippan, J. Glätzle, A. Püschel, Effect of microstructure on fatigue properties of WC-Co hard metals, Procedia Eng. 2 (2010) 2001–2010.

[24] T. Teppernegg, T. Klünsner, C. Kremsner, C. Tritremmel, C. Czettl, S. Puchegger, S. Marsoner, R. Pippan, R. Ebner, High temperature mechanical properties of WC–Co hard metals, Int. J. Refract. Met. Hard Mater. 56 (2016) 139–144.

[25] C. Kirchlechner, K.J. Martinschitz, R. Daniel, C. Mitterer, J. Keckes, Residual stresses in thermally cycled CrN coatings on steel, Thin Solid Films. 517 (2008) 1167–1171.

[26] C. Kirchlechner, K.J. Martinschitz, R. Daniel, M. Klaus, C. Genzel, C. Mitterer, J. Keckes, Residual stresses and thermal fatigue in CrN hard coatings characterized by high-temperature synchrotron X-ray diffraction, Thin Solid Films. 518 (2010) 2090–2096.

[27] M. Bľanda, A. Duszová, T. Csanádi, P. Hvizdoš, F. Lofaj, J. Dusza, Indentation hardness and fatigue of the constituents of WC–Co composites, Int. J. Refract. Met. Hard Mater. 49 (2015) 178–183.